Soft Matter

Accepted Manuscript

ROYAL SOCIETY OF CHEMISTRY

www.rsc.org/softmatter

Journal Name

RSCPublishing

ARTICLE

A thermodynamic approach to predict apparent contact angles on microstructures using surface polygonal maps

Cite this: DOI: 10.1039/x0xx00000x

Received 00th January 2012,
Accepted 00th January 2012

DOI: 10.1039/x0xx00000x

www.rsc.org/

A. Calvimontes[a]

The thermodynamic model of wetting developed and tested in this work allows the understanding and prediction of the apparent contact angles on the topographic maps of real and digitally generated microstructures. The model considers the solid component as a set of finite areal elements in the form of a polygonal map. Liquid and gas components are instead evaluated as continuous and incompressible volumes. In this study the concept of the wetting topographic spectrum (WTS) is proposed to simulate the changes in the liquid-solid contact areas and of the interfacial energies while wetting the microstructure from the top to the bottom of the topographic map, passing through various states of metastable equilibrium, to find a stable configuration. The model was successfully applied to predict the wetting apparent contact angles on randomly micro structured polypropylene (PP) surfaces and on a superhydrophobic and superoleophobic transparent polydimethylsiloxane (PDMS) microstructure previously presented as a communication in this Journal by other authors. The method presented in this study can be used to design and predict the geometry of microstructures with special wetting characteristics.

Introduction

Various theories and models have been developed in the last century to predict wetting and to understand how the roughness of a surface controls wetting. The work of Wenzel [1], Cassie and Baxter [2], Shuttleworth and Bailey [3], Good [4], the contributions of Johnson and Dettre [5], Leger and Joanny [6], Andrade et al. [7], Grundke [8], Gaydos and Newmann [9], as well as those of many other authors have elucidated the mechanisms that control the balance and dynamics of the advancing and receding contact angles of liquid droplets on rough solid surfaces.

Several authors have suggested mathematical models to predict wetting using idealized surfaces. Cassie and Baxter, and Drelich and Miller [10], for example, based their models on surfaces formed by thin parallel cylinders. Sheng et al. [11] and Ishino et al. [12] based their work on surfaces consisting of tiny elements of rectangular profile, while Extrand [13] did so using trapezoidal elements. Wolansky and Marmur [14] developed their model using triangular profiles, and Johnson and Detré developed a mathematical model for sinusoidal profiles.

Nakae et al. [15] stepped forward by making steel surfaces with thin cylinders of 50 microns in diameter. Krupelin et al. [16] studied nanostructured silicon surfaces of cylinders of 7 microns in length and 350 nanometres in diameter. Synytska et al. [17] studied surfaces of silicon hemispheres of different diameters (100 nm to 10 µm) in hexagonal arrangements. Im et al. [18] imprinted trapezoidal PDMS (polydimethylsiloxane) elements of 26 microns in diameter and 11.9 microns in height, and investigated the effects of coating this surface with a thin layer of Teflon.

The aim of this study is to propose a thermodynamic model to find the most probable contact angles by calculating the thermodynamic and physical barriers established by the topography of random and regular microstructures, including those with inwardly inclined edges and lateral interstices. This method focuses only the geometrical variability of the surfaces and assumes that the surface is chemically homogeneous.

Theoretical Basis

Topographic maps.

There are two types of topographic maps, the Cartesian and the polygonal maps. Traditionally, topographic maps have been constructed using Cartesian coordinates. The first mechanical profilometers allowed the topography measurement by moving the needle (Stylus) on the horizontal axis while simultaneously determining the height on the vertical axis. Later, the profilometers became three-dimensional detection systems by moving the Stylus on the XY axes. For that reason, topographic maps are constructed by assigning an array of three numeric values (x, y, z) to each measured position.

All topographic measurement systems have the enormous limitation of being unable to recognize the lateral cavities that are part of the surface porosity. This limitation arises from the measuring principle used, both in the mechanical and in the optical profilometry. Optical measurement systems recognize the topography up-down. Where there are lateral interstices, they can only recognize vertical edges. Mechanical profilometers have the additional limitation of being dependent on the way the geometry of the measuring pin (Stylus) interacts with the surface morphology.

If the adjacent points of a Cartesian map are joined together using line segments that generate small polygonal areas, it becomes in a polygonal map. Thus, a matrix of points can be converted into an array of small square or triangular tiles. If one uses triangles, their orientation can produce two different types of arrangements for the same surface, as Fig. 1 shows. For the correct calculation of the actual surface of a topographical map, the Cartesian map has to be transformed into a surface of triangular tiles, where then the sum of all the small areas can be calculated. Since there are two possible versions of triangle maps for each Cartesian map, the total area of both versions must be calculated, and then the arithmetic mean from both is obtained.

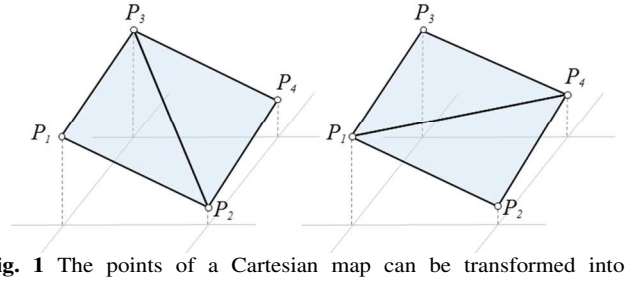

Fig. 1 The points of a Cartesian map can be transformed into a collection of triangles with two possible configurations.

Polygonal maps are essential for calculating the real area of surfaces, and especially to calculate the ratio *r* (the actual surface area divided by the area of the projected measured plane). This ratio, introduced by Robert N. Wenzel in 1936, is by definition equal or larger than one. It is the most valuable topographic parameter in wetting theories because it expresses the increase or decrease of the area and thus the increase or decrease of surface and interfacial energy.

The calculation of the ratio *r* is practically the only application of polygonal maps derived from the current Cartesian maps. However, the rapid development of computational techniques for generating three-dimensional objects now makes possible the use of polygonal maps for evaluating the physical properties of surfaces with inwardly inclined edges and lateral interstices such as those illustrated in Fig. 2. The maps in this illustration have been digitally generated because, although they are much better representations of natural surfaces, their capture is nowadays not possible using the mechanical or optical methods available for topographic analysis.

From a mathematical standpoint, the main difference between a Cartesian and a polygonal map is that, while in the Cartesian map there is only one value of z for each pair (x, y), in a polygonal map a pair (x, y) can have several z values.

Many computer techniques have been developed in the last years for the manipulation of three-dimensional objects including many matrix arrays to generate, transform and store polygonal surfaces. These virtual objects are mostly used by the digital entertainment industry and, in fact, many of the programs and algorithms used in this study to handle polygonal maps come from the digital animation industry. In the future it may be possible to capture three-dimensional images of the surface with inwardly sides and lateral interstices. All the characterization techniques shall then be reviewed and updated, as well as the algorithms and evaluation programs, because currently, practically all of them are based on Cartesian maps.

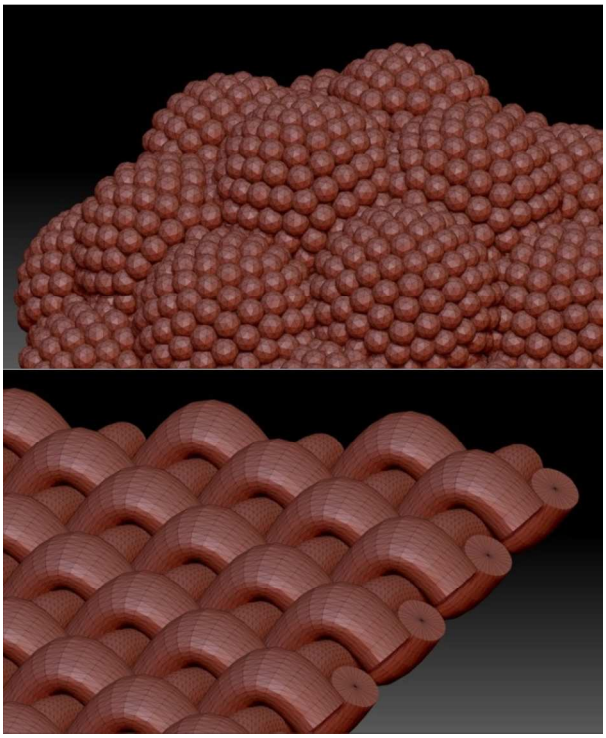

Fig. 2 Digitally generated polygonal maps. Above: fractal arrangement of spherical elements constructed using the film animation software Houdini FX (Side Effects Software Inc., Canada). Below: woven plain fabric made of monofilament yarns, generated by the virtual material laboratory GeoDict 2012 R1 (Math2 Market GmbH, Germany). Both images displayed using ZBrush 4R6 software (Pixologic Inc., USA).

Topography and wetting

The angle formed by the contour of a drop on a completely flat solid surface is called the intrinsic contact angle or Young's contact angle θ_Y [8] (Fig. 3). Young's equation represents the balance of forces in equilibrium at a specific point of the contact line:

$$\gamma_{LG}\cos\theta_Y = \gamma_{SG} - \gamma_{SL} \qquad (1)$$

where γ_{LG} is the surface tension of the liquid, γ_{SG} is the surface energy of the solid, and γ_{SL} is the energy of the liquid-solid interface. According to this model, the tensors γ_{SL} and γ_{SG} are intrinsic properties that depend on the chemical properties of the surface. If γ_{SG} - $\gamma_{SL} > 0$, the contact angle is less than 90° (hydrophilic surface), whereas if γ_{SG} - $\gamma_{SL} < 0$, then $\theta_Y > 90°$ (hydrophobic surface).

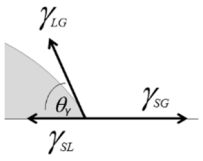

Fig. 3 Young's equation represents the balance of forces in the contact line of the solid, liquid and gaseous phases.

Wetting replaces an area of the gas-solid interface by an equivalent area of a solid-liquid interface. This effect is usually accompanied by changes in the area of the liquid-gas interface. These surface relationships vary with the system's conditions and can change during the wetting process depending on the topography. Since each interface has its own specific surface energy, the result is a net increase or decrease of the total interfacial energy. From the standpoint of thermodynamics, the magnitude of the change in Helmholtz energy (described below) determines whether wetting will proceed spontaneously and how fast and how far it can go against the external forces that oppose the process or how large the external force must be to overcome the resistance to wetting. The first study of the wetting phenomena on rough surfaces was conducted by Wenzel in 1936 and later supplemented by Cassie and Baxter in 1944. Wenzel assumed that the liquid wets all the solid irregularities, and generalized Young's equation for the Wenzel's contact angle ϕ_W:

$$\cos\phi_W = r\cos\theta_Y \qquad (2)$$

where r is 'Wenzel roughness factor' or simply 'Wenzel roughness', a quantity defined as the ratio between the actual and the projected areas. This factor is equal to one for completely flat surfaces and is greater than one for rough surfaces. If $\theta_Y < 90°$, an increase in roughness results in improved wetting because the value of $\cos\phi_W$ increases and, therefore, ϕ_W decreases. Conversely, when $\theta_Y > 90°$ and r increase, the apparent angle ϕ_W becomes even greater. In other words, in Wenzel's regime, an increase in roughness transforms an hydrophobic surface into an even more hydrophobic one, and a hydrophilic surface into an even more hydrophilic one. In practice, however, this model is only used for hydrophilic surfaces ($\theta_Y < 90°$), because in the rough hydrophobic surfaces the liquid cannot wet the whole surface due, aside from the thermodynamic reasons, to the presence of air pockets. In this case, then the main requirement of Wenzel's regime, complete wetting, would not be fulfilled.

Therefore, eight years later, Cassie and Baxter considered wetting a homogeneous substance with two different surface energies. In this case, the Cassie-Baxter apparent contact angle ϕ_{CB} is given by:

$$\cos\phi_{CB} = f_1\cos\theta_1 + f_2\cos\theta_2 \qquad (3)$$

where f_1 is the total area of solid-liquid interface, also called solid fraction, and f_2 is the total area of liquid-air interface in a plane geometrical area parallel to the rough surface. θ_1 and θ_2 represent the intrinsic contact angles of components *1* and *2*, respectively.

Porous surfaces can be considered as being composed of a solid fraction and pores filled with air, i.e. the surface roughness is saturated with air. If this surface becomes in contact with a liquid, the saturated air pores can then be regarded as the component with $\theta_2 = 180°$, which is the air-liquid contact angle. Because $\cos\theta_2 = -1$, Eq. (3) can be written as:

$$\cos\phi_{CB} = f_1\cos\theta_1 - f_2 \qquad (4)$$

According to Eq. (4), if the hydrophobicity given by ϕ_{CB} and the fractions f_1 and f_2 are appropriately combined, a drop of water deposited on a superhydrophobic surface could remain nearly spherical.

With the exception of Wenzel's roughness r and the fractions f_1 and f_2, the theories of Wenzel and Cassie-Baxter are essentially independent of the geometric characteristics of roughness, i.e. the shape of the pores.

If the liquid penetration into a porous surface by capillary forces is not present, wetting is usually associated with either the regimes of Wenzel or of Cassie-Baxter. It is normally assumed that if $\theta_Y < 90°$ Wenzel regime is met, while if $\theta_Y > 90°$ the Cassie-Baxter regime is met. However, the experimental results sometimes show that this criterion is not completely correct. From a thermodynamic standpoint the best approach is that the most stable configuration –the equilibrium state- corresponds to the greatest change during the decrease of Helmholtz energy while wetting.

By definition, surface tensions, such as surface and interfacial energies, are related to one unit of the actual area. However when a liquid spreads over the surface of a real solid, the forces that oppose each other along a given length of the advancing periphery of the wetted area are proportional in magnitude, not to the surface tensions of the respective interfaces, but to their total energies per unit of geometric surface (it must be true if surface tensions themselves are characteristic properties, unaltered by surface roughness). As consequence of this reasoning, the topography of the surface plays a crucial role in the wettability. During the simulation of wetting, the surface energy values must be constantly adjusted depending on the actual extent of the surface, i.e. Wenzel's roughness.

The aim of this Section is to develop a thermodynamic model to predict the most probable thermodynamic configuration during wetting of real rough surfaces, starting with the equations of Wenzel and Cassie-Baxter, and thus to predict the most probable angles that formed by a drop of liquid in the contact line with a solid surface, the so-called apparent contact angles. For this purpose, it is necessary to begin by describing the components of the system: the solid surface, the intrinsic contact angle (Young's angle), the apparent contact angles, the possible hysteresis of contact angles, the metastable thermodynamic configurations, the contact areas and the discrete positions for the metastable equilibrium.

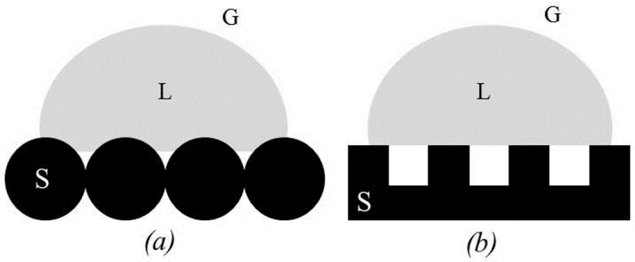

Fig. 3 a) Scheme for Cassie-Baxter model. b) Erroneous simplification of the Cassie-Baxter model.

Cassie and Baxter assumed that the total contact area formed by the liquid interface with a rough solid and the gas inside its pores is given by $f_1 + f_2 > 1$. However, this value is lower than the total interface of the solid with the liquid and the gas inside the pores, which is given by Wenzel roughness r, i.e. $f_1 + f_2 < r$. Cassie and Baxter validated their theory studying a surface of horizontally aligned fibres (cylinders), as shown schematically in Fig. 3-a. Later, some authors interpreted that $f_1 + f_2 = 1$ and reduced the Cassie-Baxter model to a very simple idealization that can be presented as the rectangular profile of Fig. 3.b. In this simplification, the liquid does not penetrate into the pores.

For the purpose of this study, it is necessary, to combine Eq. (2) and Eq. (3) in a single general expression. Let's take as the

starting point the reasoning of Cassie and Baxter (Fig. 4) and call ϕ the apparent contact angle; f_s the surface fraction of the solid-liquid interface with respect to the total surface of the solid (f_1 of Cassie-Baxter model); f_G surface fraction of the liquid-air trapped inside the pores interface with respect to the projected area (f_2 of Cassie-Baxter model); θ_Y the intrinsic contact angle (Young's angle) of the solid; and θ_G the intrinsic contact angle of air. Then:

$$\cos\phi = f_S \cos\theta_Y + f_G \cos\theta_G \quad (5)$$

$$f_S = f\ r \quad (6)$$

where f is the fraction of the contact surface solid-liquid with respect to the projected area and r is Wenzel's roughness factor. As $f + f_G = 1$ and $\theta_G = 180°$, then:

$$\cos\phi = f\left(r\cos\theta_Y + 1\right) - 1 \quad (7)$$

which is a general expression for the Cassie-Baxter and Wenzel regimes. If the surface is perfectly flat, then $f = r = 1$, and the apparent contact angle ϕ equals Young's angle. If the solid-liquid contact is complete but on a rough surface, then $f = 1$ (complete wetting) and $r > 1$, which reduces Eq. (7) to Eq. (2), corresponding to Wenzel's regime.

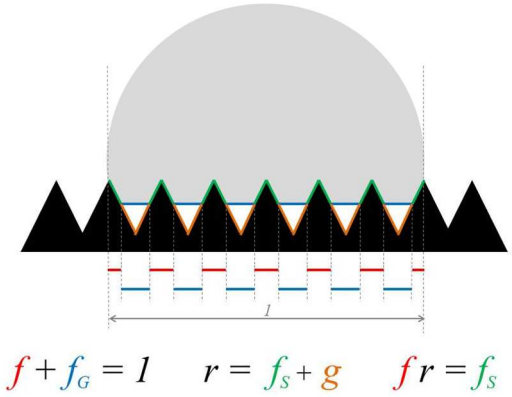

Fig. 4 Two-dimensional representation of the general model of wetting. The three relations between the dimensionless expressions f, f_G, f_S, g and r are also valid for a three-dimensional surface if they are used as areas instead perimeters. In this case, f_s represents the wetted area (f_1 in the Cassie-Baxter model), g is the surface area of the not wetted pores, r the total available area of the solid; f is the projection of f_s on the horizontal plane, and f_G the projection of g. In turn, f_G is the fraction f_2 of the Cassie Baxter-model.

The Wetting Topographic Spectrum (WTS)

Any topographic map can be used to calculate variables that control the appearance of wetting thermodynamic barriers. The numerical behaviour of these variables is the WTS of the surface.

The starting point for the construction of the WTS is the curve of the solid-liquid contact area, $\Omega_{SL(h)}$. This curve starts when the liquid touches the highest peak of the rough solid in Z_{max} and ends, if wetting is complete, in Z_{min}, when the liquid has completely wetted the surface and the contact area takes the value Ω_T.

To construct the curve $\Omega_{SL(h)}$ it is necessary to convert the Cartesian map into a polygonal one, and to calculate the surface area above different height levels h.

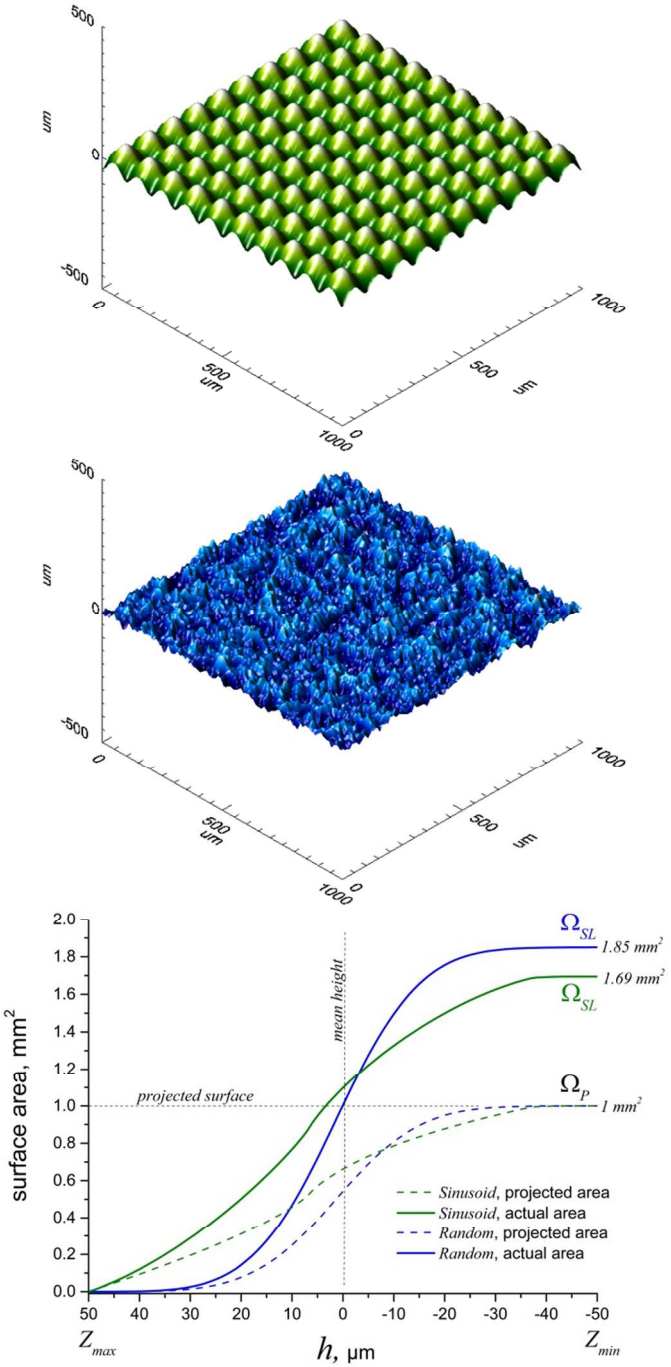

Fig. 5 Curves of surface increase, $\Omega_{SL(h)}$ and $\Omega_{P(h)}$ for the topographic maps *Sinusoid* and *Random*. The topographic maps are displayed using FRT Mark III analysis software (Fries Research & Technology GmbH, Germany).

That area is the sum of all the triangular areas of the polygonal map existing above the plane delimited by h. A good algorithm for this calculation should consider that some triangles are sectioned by the height plane resulting in fractioned triangles and trapezoids, the surface of which must be included in the sum. As mentioned above, in the calculation of the surface area there are two possible versions of polygonal maps, each one with differently oriented triangles, as shown in Fig. 1. The correct evaluation of $\Omega_{SL(h)}$ has to take into account the arithmetic mean of both polygonal map versions.

$\Omega_{SL(h)}$ is calculated for each height, i.e. for each position of the liquid as it moves from top to bottom during wetting. At the same time, one must calculate the curve corresponding to the increase of the wetted surface, $\Omega_{P(h)}$, projected on the horizontal plane. An alternative simple method for this purpose is the use of the Abbott-Firestone curve [19-22], which is a cumulative density function of surface area. In the topographic characterization, the Abbott-Firestone curve is expressed as the curve of percentage frequency against height. Commercial topographic evaluation software usually build this curve quickly and efficiently as a cumulative distribution curve of heights using Cartesian instead of polygonal maps.

To construct the curve of surface increase it is recommendable to give the mean height (the average of all the measured heights) the value zero. Thus, the vertical range of the surface will be given by a positive value of Z_{max} in the tallest peak and a negative value of Z_{min} in the deepest cavity.

Previously (see Eq. 6), r was defined as:

$$r = \frac{f_S}{f} = \frac{\Omega_{SL}}{\Omega_P} \qquad (8)$$

where, in a topographic map, Ω_P is equal to the measured area L_m^2. Fig. 5 shows the curves $\Omega_{SL(h)}$ and $\Omega_{P(h)}$ for two topographic maps, a sinusoidal map and a random surface map, both digitally generated with N x N = 1000 x 1000 points, L_m = 1000 µm, Z_{max} = 50 µm and Z_{min} = -50 µm. The same conditions were used to generate the topographic maps of Figs. 6-8, which show the effect of the morphology on the increase of the surface area.

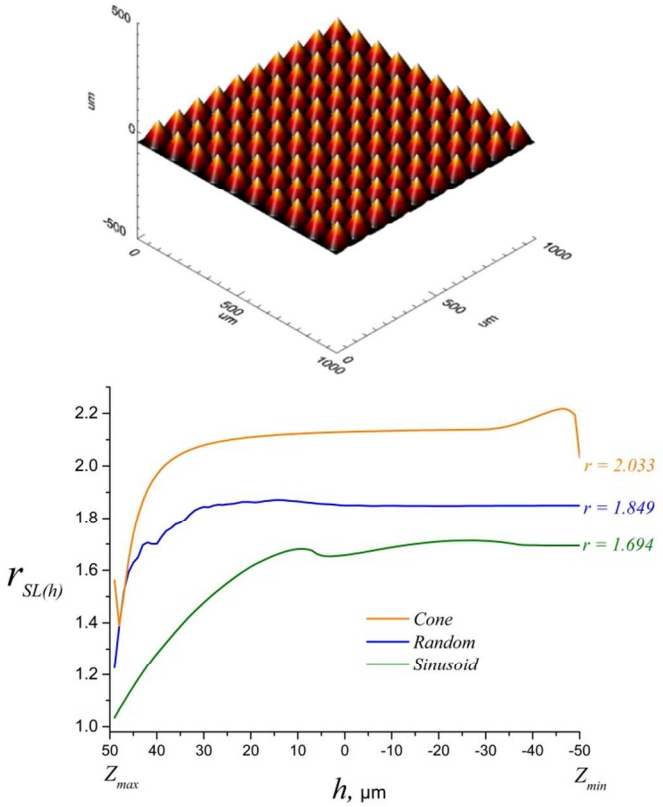

Fig. 6 Above: topographic map of *Cone* surface. Below: roughness curves for *Random*, *Cone* and *Sinusoid* maps. Reaching Z_{min} all the curves converge to the r value of the topographic map.

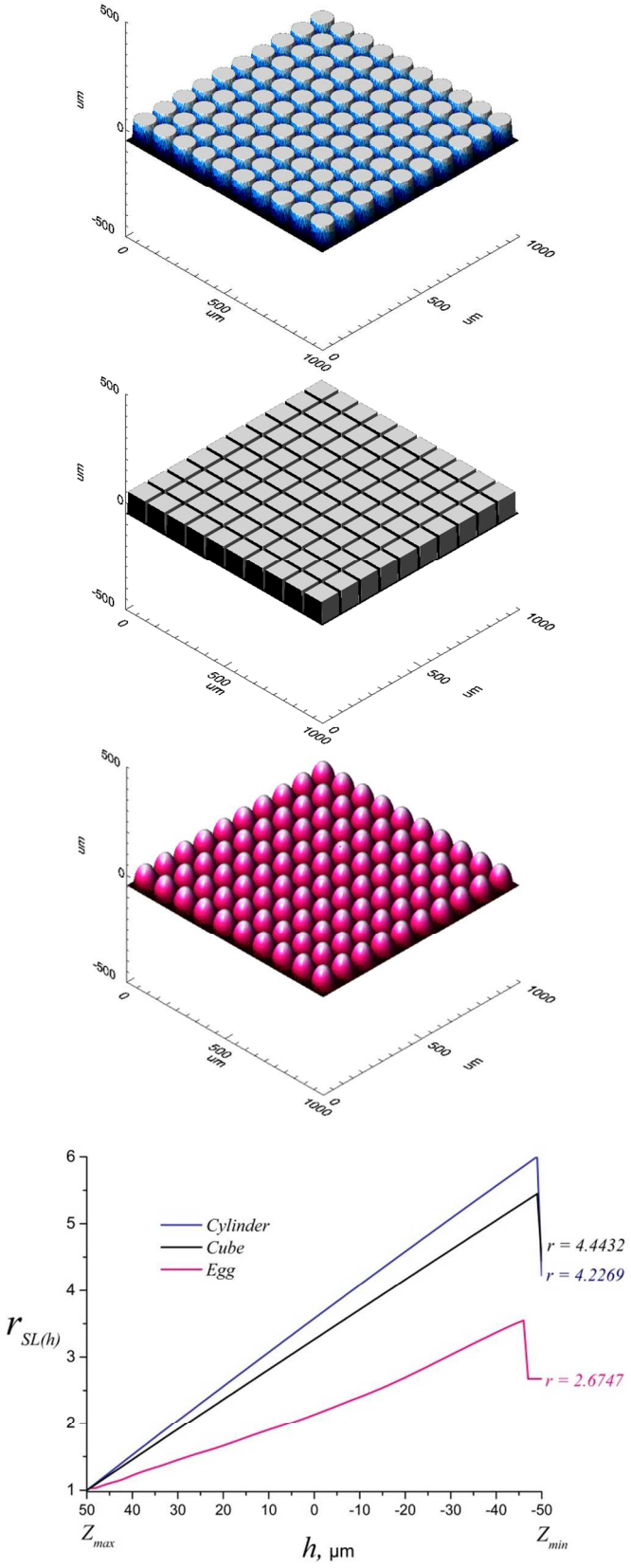

Fig. 7 Roughness curves for three different topographic maps. Linear increases of *Cylinder* and *Cube* are due to their vertical edges. The topographic maps are displayed using FRT Mark III analysis software.

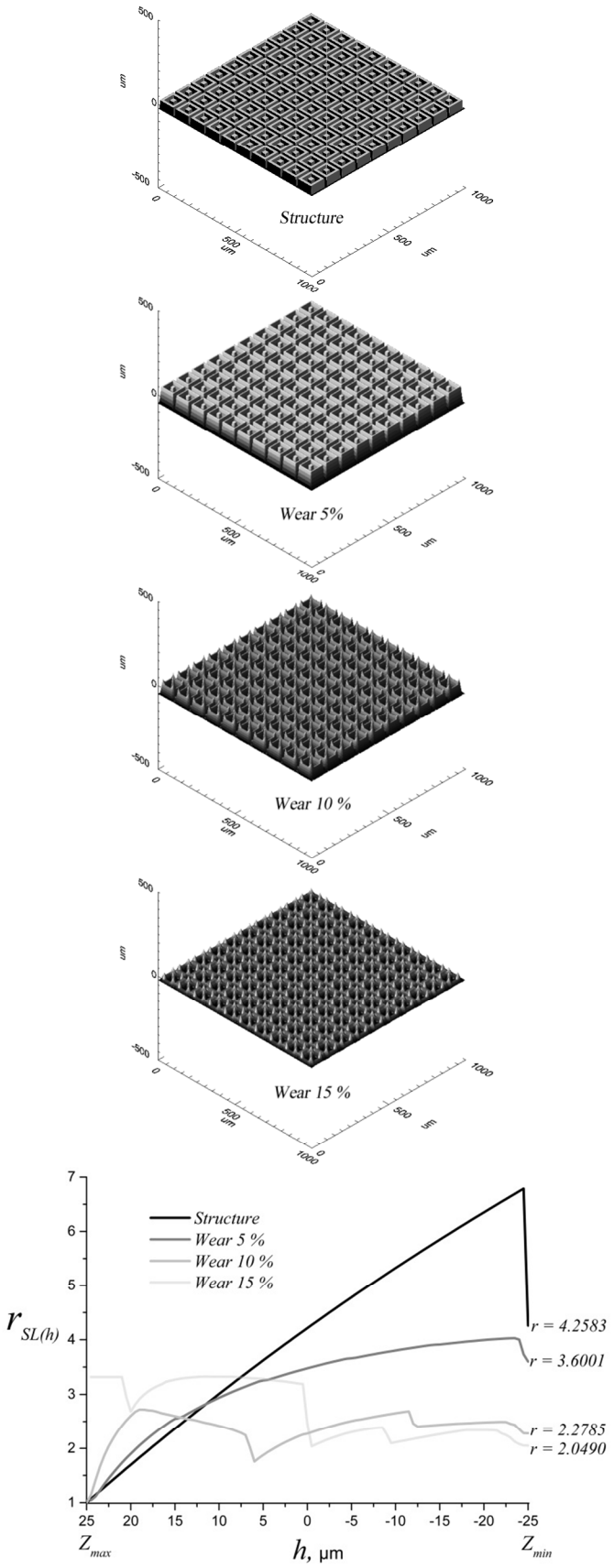

Fig. 8 Decay of the roughness curve of a vertical profiles structure by applying a mathematical smoothing filter at different intensities.

In 1998 Good et al. [23] developed a mathematical model to obtain the *r* value of a nonpolar surface without its topographic information. They found a correlation between an algebraic expression for the interfacial energy and the apparent contact angle and then successfully applied their model to Teflon surfaces modified using different sandpapers. According to the concepts presented in this Section, the *r* values found by Good and his colleagues do not correspond to the whole Teflon surface but only to the fraction where the solid is in contact with the liquid.

Traditionally, only one *r* value has been considered for each solid surface, as Good et al. did, however, *r* is not constant during the wetting process. The increase of the contact area $\Omega_{SL(h)}$ and its projection on the horizontal plane $\Omega_{P(h)}$ results in the roughness curve $r_{SL(h)}$ (Figs. 6-8) by means of:

$$r_{SL(h)} = \frac{\Omega_{SL(h)}}{\Omega_{P(h)}} \tag{9}$$

When the curve reaches Z_{min}, the numerator of the right side of Eq. (9) becomes Ω_{SL}, the denominator L_m^2 and the resulting value of $r_{SL(Zmin)}$ is *r*: Wenzel's surface roughness , as seen in Eq. (8).

So, Eq. (6) can now be expressed as the following equations:

$$f_{S(h)} = f_{(h)}\, r_{SL(h)} = \frac{\Omega_{SL(h)}}{L_m^2} \tag{10}$$

$$f_{(h)} = \frac{\Omega_{P(h)}}{L_m^2} \tag{11}$$

As stated above, $f_{S(h)}$ and $f_{G(h)}$ are the solid-liquid and the liquid-gas contact fractions respectively, both with respect to the total projected area. As can be seen in Figs. 6-8, $r_{SL(h)}$ increases as the liquid level advances from Z_{max} to Z_{min}. This increase, however, is not linear as it depends on the surface morphology and, in many cases, has a maximum value. Finally, at the complete wetting, in level Z_{min}, $r_{SL(h)}$ equals Wenzel's roughness of the topographic map.

In Fig. 7, the roughness curves *Cylinder* and *Cube* are linear due to their vertical edges. The largest vertical areas of *Cube*, present a much larger projected area while moving the height level from top to bottom, therefore, its maximum $r_{SL(h)}$ value is below that of *Cylinder*. Reaching the bottom of the topographic map all curves decrease sharply due to the sudden increase of the projected area.

The roughness curve is the main component of the WTS because it controls the wetting equilibrium of rough surfaces, as will be seen below. This curve is very sensitive to the morphologic changes that can occur due to external agents, such as mechanical wear, for example. Fig. 8 shows how the roughness curve of the surface *Structure* decay by applying a digital smoothing filter [20] at different intensities (*Wear 5 %, 10 %* and *15 %*).

As mentioned, the roughness curve $r_{S(h)}$ is the first component of the WTS. The second component is $.r^*_{(h)}$, the average of all the local Wenzel roughness factors of the polygons in the solid-liquid contact line, One straightforward way to construct this curve is by the following equation can be used:

$$r^*_{(h)} = \frac{r_{SL(h)}\, f_{(h)} - r_{SL(h-\Delta h)}\, f_{(h-\Delta h)}}{f_{(h)} - f_{(h-\Delta h)}} \tag{12}$$

$r_{SL(h)}$ and $r_{SL(h-\Delta h)}$ can be calculated for each height using the set of points obtained from the Eq. (9) , while $f_{(h)}$ y $f_{(h-\Delta h)}$ can be obtained from the Abott-Firestone curve. For more accuracy, at any given height, it is possible to obtain $r^*_{(h)}$ by calculating $r_{SL(h)}$ and $f_{(h)}$ using the upper and lower intervals, $(h+\Delta h)$ and $(h-\Delta h)$, respectively. However, building a WTS using small values of Δh in the Eq. (12) is more than enough.
Fig. 9 shows the mean slope curves, $r^*_{(h)}$, for the topographic maps *Cone*, *Random* and *Sinusoid*.

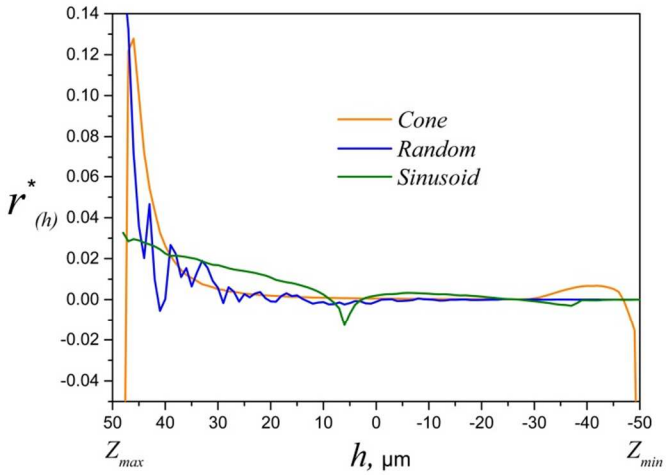

Fig. 9 Mean slope curves of surfaces *Cone*, *Random* and *Sinusoid*.

The WTS is complete with the information regarding the peaks and cavities of the surfaces. For the morphologies *Cone*, *Cylinder*, *Egg* and *Structure*, the peaks count curves present only a constant value that corresponds to the number of geometrical elements per unit area, and there is only one cavity whose volume decreases as the height level decreases. For the *Sinusoid* surface, there is a constant number of peaks per unit area, but the number of cavities starts being one and gets fractionated near the mean height.

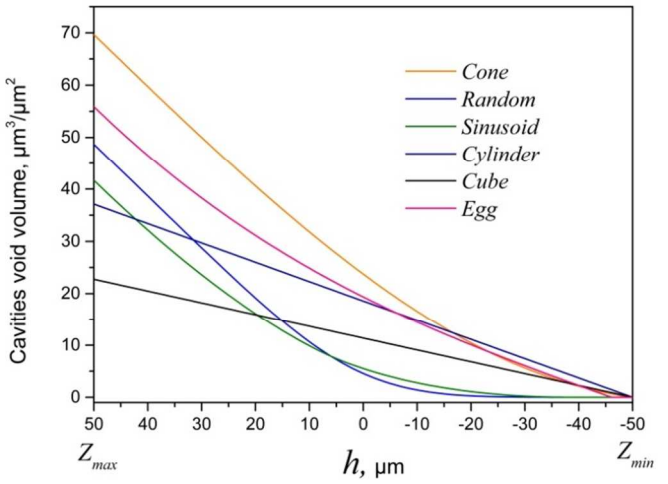

Fig. 10 Void volume curves of different surface morphologies.

An additional parameter for the WTS spectrum, especially useful for characterising surfaces of idealized morphology, is the void volume curve under the line of wetting (Fig. 10). Commercial topographic evaluation programs typically use the Cartesian map to calculate the number of voxels, i.e. cubic pixels of side Δx and height equal to the vertical resolution, with which they easily and efficiently estimate the volumes between the wetting threshold and the solid surface.
The void volume decrease is completely linear for surfaces with vertical edges. Void volume curves characterize the surface morphology and, in practice, are independent of the resolution used to obtain the topographic map.

Apparent and intrinsic contact angles

To construct the thermodynamic model, it is necessary to assume that the drop volume is constant, that it wets the surface with a constant intrinsic angle θ_Y, and that there are no gravitational forces present. Also, the liquid is one-component, and the solid is insoluble in the liquid. Finally, it must be assumed that the surface roughness, both in amplitude and distance between neighbouring peaks, is negligible compared to the radius of the liquid drop.
In [3], Shuttelworth and Bailey established that the experimental angles at a topographic level h, also called apparent angles $\phi_{(h)}$, are given by the sum or the by difference of the intrinsic angle θ_Y and the angle $\alpha_{(h)}$ of the surface slope at the liquid-solid contact point, as shown in Fig. 11. Then:

$$\phi_{(h)} = \theta_Y \pm \alpha_{(h)} \qquad (13)$$

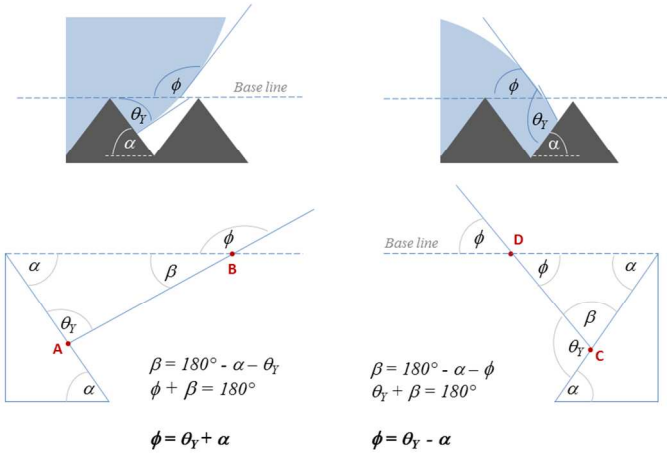

Fig. 11 Schematic representation and solution of the larger and smaller apparent contact angles. The arcs AB and CD are so short that can be considered line segments.

Eq. (13) is valid only if AB and CD in Fig. 11 are so short that they can be assumed to be line segments. In other words, the roughness of the surface is negligible compared with the radius and curvature of the drop.
According to Fig. 11:

$$\tan \alpha_{(h)} = \left| \frac{\partial z}{\partial x} \right| \qquad (14)$$

$$\cos \alpha_{(h)} = \frac{1}{r^*_{(h)}} \qquad (15)$$

Thus, to make it simpler, there will be always a positive slope but two different values for $\phi_{(h)}$. In practice, there are two apparent angles along the contour of the drop line and the rough

surface, but the larger one masks the smaller when measuring the contact angle using optical or digital goniometers, i. e., the apparent contact angle of the drop on a solid surface can be expressed as the sum of $\phi_{(h)}$ and $\alpha_{(h)}$. As demonstrated in [24], while studying dynamic contact angles and wetting hysteresis of irregular polypropylene surfaces modified by different sandpaper grits, the larger angle can be also associated with the advancing contact angle ϕ_a, while the smaller angle can be associated with the receding contact angle ϕ_r, however the true advancing and receding contact angles are also dependent on the chemical hysteresis that is independent of the surface roughness.

Thermodynamic potential of metastable configurations

In the analysis of metastable configurations an important element is the difference in the Helmholtz free energy between two configurations of the system [5]. The term "configuration" refers to a state in which the drop of liquid is at rest in a position of metastable equilibrium. Associated with each configuration are a characteristic contact angle and a characteristic Helmholtz free energy. In thermodynamics, the Helmholtz energy is a potential that measures the "useful" work obtainable from a closed system. The negative of the difference in Helmholtz energy is equal to the maximum amount of work that the system can perform in a thermodynamic process in which the temperature is held constant. Therefore, the condition for spontaneous change is that the difference in Helmholtz energy is less than zero.

According to this, the most probable configuration is obtained by comparing the Helmholtz energies of adjacent, infinitesimally close states (heights), which are all in metastable equilibrium.

To construct a model on a sinusoidal profile, Johnson y Dettre [5] used cylindrical coordinates and considered the energy of the entire surface of the liquid drop, not only the surface forming the interfaces with the solid and with the air inside the pores of the solid, but also that of the upper drop hemisphere formed by the liquid in contact with air. This practice of considering the entire volume of the drop in wetting models has also been followed by other authors in the past [23]. Considering the large contact area between the drop and the air, the volume of the drop contributes significantly to the total surface energy of the system, so that in many cases the interfacial energy between solid-liquid and liquid-air (between liquid and the air inside de pores), are negligible compared to that provided by the upper hemisphere of the liquid drop. By cancelling the gravitational force, Good et al [23] have attempted to eliminate the dependence on drop volume. However, even though the water pressure on the surface is small, the high surface tension of some fluids, such as water, causes the volume of the drop to be decisive during the calculation of the system equilibrium. Therefore, it is necessary to define the system for the simulation so that the outer surface of the drop is not part of it, making the drop volume irrelevant. In the laboratory, at the same time, for the gravitational force and the pressure of the liquid on the surface to be negligible, the experimental drop volumes must be small, only about five to ten microliters.

The system is then defined by a parallelepiped volume **V** in the contact area of the drop with the surface, as shown in Fig. 12. This small continuous volume has the size L_m x L_m x (Z_{max} – Z_{min}) and contains the solid surface, the columns of liquid in contact with the solid (only up to the highest point of the solid), and the air trapped between the solid and liquid. In practice, **V** can correspond to the three-dimensional space captured by a topographic measurement or generated by computer software. The apparent and intrinsic angles inside this volume are exactly those of the outer contour line of the droplet in contact with the porous solid. As the drop volume is very small, the liquid column does not exert any pressure on the solid or on the air trapped inside the solid cavities.

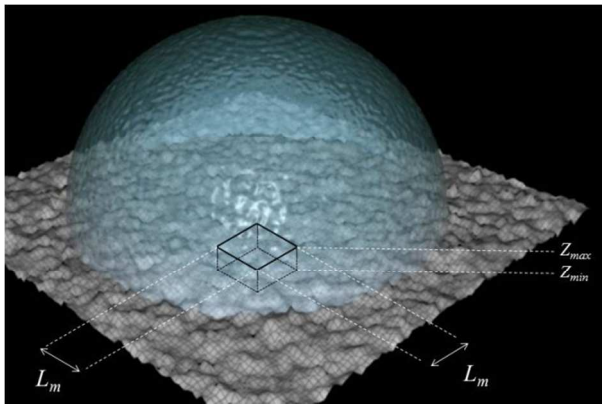

Fig. 12 The solid-liquid-gas system for the model is defined by the volume **V** with sizes L_m x L_m x (Z_{max} - Z_{min}) in the contact region between solid and liquid.

Under these considerations, the Helmholtz energy in **V**, for each wetting level, is given by:

$$A_{H(h)} = A_{L(h)} + A_{SL(h)} \tag{16}$$

where $A_{L(h)}$ is the work obtainable from the interface formed by the liquid with the air inside the pores at the height level h, and $A_{SL(h)}$ is the work obtainable from the interface formed between the liquid and the wetted parts of the solid surface from the level Z_{max} to h.

$A_{SL(h)}$ can also be expressed as the work necessary for the liquid to wet the solid, so:

$$A_{SL(h)} = -W_{SL(h)} \tag{17}$$

where $W_{SL(h)}$ is the work of wetting from Z_{max} to h.

In order to develop the expressions (16) and (17) it is necessary to know the areas of the solid-liquid and liquid-air interfaces inside the pores of the solid. This information is provided by the WTS.

A relatively simple way to get the value of $A_{SL(h)}$ for a given wetting level, is by the product of the surface energy given by (γ_{SL} - γ_{SG}), and the area of the solid-liquid interface $\Omega_{SL(h)}$:

$$A_{SL(h)} = \left(\gamma_{SL} - \gamma_{SG}\right) \Omega_{SL(h)} \tag{18}$$

From Eq. (10):

$$\Omega_{SL(h)} = L_m^2 \, f_{(h)} \, r_{SL(h)} \tag{19}$$

where, as described above, $r_{SL(h)}$ is the roughness function of the wetted surface only.

In the study of roughness and wetting, it has been traditionally considered that at a defined length-scale, each surface has only one Wenzel roughness value. This practice is correct only in the case of complete wetting, i.e., the Wenzel regime. However, if

some parts of the solid are not wetted, it tone must be rigorous during the calculation of the wet areas, which are crucial for the equilibrium configuration.

If a surface with a triangular profile, like the one shown in Fig. 4, is wetted from top to bottom, the size of the solid-liquid interface increases linearly. This is because the slope is always the same at any point in the surface. That is the procedure that Johnson and Dettre [5] followed in their model for a sinusoidal profile surface: they calculated the wetted area by multiplying the solid fraction $f_{(h)}$ by the Wenzel roughness r, which was assumed constant in all the height range. However, in many idealized, and especially in real surfaces, Wenzel's roughness is not the same in all height ranges because of differences in morphology and, therefore, the gradients are not constant. In these cases, which in practice are almost all, the partial values of Wenzel roughness for all the height levels, i. e. the $r_{SL(h)}$ values, will be provided by the WTS.

Combining Eq. (18) and (19) with (1), results in:

$$A_{SL(h)} = -\gamma_{LG} \cos\theta_Y L_m^2 f_{(h)} r_{SL(h)} \quad (20)$$

where, as already stated, $f_{(h)}$ and $r_{SL(h)}$ are dependent on the height of the solid-liquid contact line. During the wetting process from top to bottom, $A_{SL(h)}$ will change as a function of $f_{(h)}$ and $r_{SL(h)}$.

The work obtainable from the liquid-air $A_{L(h)}$ contact area is more easily calculated with a simple trigonometric consideration to take into account the mean curvature of the meniscus described by the liquid above the air saturated pores. $A_{L(h)}$ is equal to the product of the surface tension of the liquid and the area of the liquid-air interface $\Omega_{LG(h)}$:

$$A_{L(h)} = \gamma_{LG} \Omega_{LG(h)} \quad (21)$$

Where:

$$\Omega_{LG(h)} = \left(1 - f_{(h)}\right) L_m^2 M_{(h)} \quad (22)$$

$M_{(h)}$ is a factor greater or equal to one. This factor corrects the area of the liquid-air interface so that the increase due to the curvature of the meniscus is taken into account, at least roughly, irrespective of whether it is oriented up or down. From Fig. 13, it can be concluded:

$$\delta_{(h)} = \theta_Y + \alpha_{(h)} - 180° \quad (23)$$

$$M_{(h)} = 2 - \left|\cos\delta_{(h)}\right| \quad (24)$$

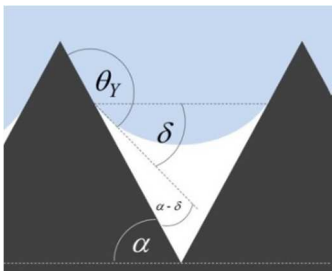

Fig. 13 The meniscus curvature of the liquid in the partially wetted pores increases the liquid-air interface. The diagram illustrates Eq. (23) which was used to estimate the meniscus related increase of the interfacial area.

So, if Young's angle is 90° and the slope is 45°, due to its curvature, the area of the meniscus would be 29 % larger. For a slope of 90° and Young's angle of 110 °, the interface would be 6 % greater. In the hypothetical extreme case that Young's angle is 90° and the slope is completely vertical (90°), then $M_{(h)}$ = 1. Considering the function $M_{(h)}$, the work obtainable from the liquid-air contact area can be calculated by:

$$A_{L(h)} = \gamma_{LG} \left(1 - f_{(h)}\right) L_m^2 \left(2 - \left|\cos\delta_{(h)}\right|\right) \quad (25)$$

Eq. (16) can be used to find the Helmholtz energy at each height; this equation is in turn the result of the sum of Eq. (20) and (25). These equations allow the calculation of the energy inside the volume **V** of the system, which has a base size L_m^2. However, to compare and plot these values it is recommended to use a reference area of one square meter, in order to be consistent with the typical units used for interfacial energy (J/m^2).

During spontaneous wetting, the Helmholtz energy changes while going through the various metastable states to find the most probable configuration. This position will be reached when the Helmholtz energy presents the highest rate of decline. In practice, this point can be found in the level corresponding to the minimum of the derivative with respect to the height, $A^*_{(h)}$. At the height h, there is a defined angle α associated with this configuration that, in turn, defines the larger and the smaller contact angles, see Fig. 11. As mentioned before, both angles coexist along the whole solid-liquid contact line, but the larger contact angle masks the smaller one, resulting in apparent (measured) contact angles close to the advancing contact angles predicted by the model.

From a thermodynamics point of view, the transition from the most probable configuration to the complete wetting, assuming that no air pockets are present, is a barrier crossing event [25]. For this reason, the most probable configuration calculated by the present model can be also considered an energy barrier of wetting.

Results and Discussion

The application of the thermodynamic model to digitally generated regular surfaces results in different equilibrium configurations and predicted contact angles when using the information provided by the changes in the Helmholtz energy while wetting with water (γ_{LG} = 72 mN/m), and the intrinsic contact angle θ_Y = 100°, as shown in Fig. 14. The topographic maps analysed in this study correspond to *Random*, *Sinusoid*, *Cone*, *Cylinder* and *Egg* morphologies, presented above, but with a maximum amplitude of 50 microns (Z_{max} = 25 µm, Z_{min} = -25 µm).

In the *Random* morphology during the first contact with the liquid- immediately below Z_{max}- the surface shows a region of non-equilibrium states, characterized by jumps in the Helmholtz energy, . Close to the mean height, a region of metastable equilibrium (Fig. 14) and a physical barrier (air saturated cavities), approximately 6 microns below that level, can be observed; this physical barrier corresponds to the maximal cavities count of the WTS. In contrast, the *Sinusoid* topographic map shows metastable equilibrium 3 microns above the mean height and the physical barrier exactly at the mean height, where the surface is fractionated into many air saturated cavities. The *Cone* and *Egg* morphologies in turn, show their most probable configurations exactly 2.5 microns below Z_{max}, although with different contact angles because of

the morphological differences between them. In this case, the advancing contact angle on the *Cone* surface is larger due to its larger slope near Z_{max}. According to the model, the liquid would never penetrate inside the *Cylinder* and *Cube* surfaces (ϕ_a = 180°) due to their vertical edges. Unfortunately, such ultra-hydrophobic surfaces exist only as idealizations or as digitally generated objects because these surfaces, made of completely vertical and clean edges, cannot exist in the real world. The *Cone*, *Cylinder*, *Egg* and *Cube* morphologies have no physical barriers during wetting because the air inside the cavities can escape anytime without becoming trapped inside pockets. In the virtual surface *Structure* (Fig. 8), however, the virtual ultra-hydrophobicity is due not only to the completely vertical and clean edges, but also to the presence of air saturated cavities at the beginning of wetting in Z_{max}.

In practice, to obtain the most probable apparent contact angle, one must first find the value of h at the most probable configuration, using the Helmholtz derivative curve, and then the value of $r^*_{(h)}$, using the curve generated by Eq. (12). In turn, $\alpha_{(h)}$ be obtained by Eq. (15). The apparent advancing and receding contact angles can be calculated using Eq. (3).

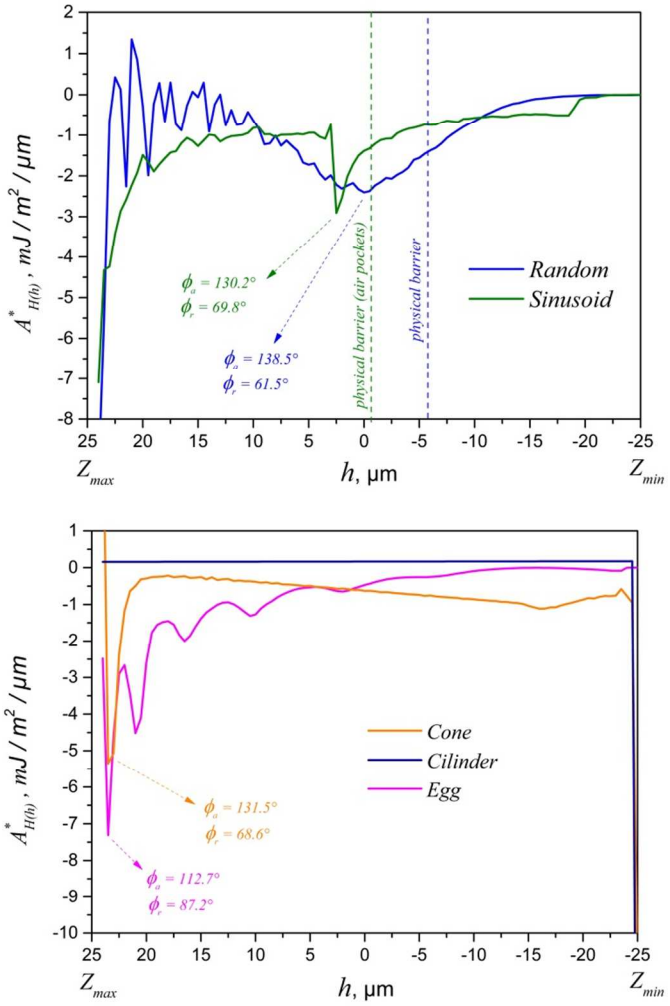

Fig. 14 The minima of the curves indicate the maximum decrease in Helmholtz energy. The simulated contact angles at the most probable metastable configuration equilibrium correspond to water (γ_{LG} = 72 mN/m), using a material surface with θ_Y = 100°.

In order to verify the effectiveness of the model using real random morphologies, a PP surface was mechanically structured using sandpapers of different grits (600, 1500, 3000, 6000 and 12000). The topography of each resulting surface was measured on three different positions using the confocal microscope µsurf explorer (Nanofocus AG, Germany). Three different optical objectives were used: 20X, 60X and 100X, which provide measure lengths (L_m) of 800 µm, 260 µm and 160 µm respectively. The lateral resolutions (Δx) associated with each optical objective were 1.5 µm, 0.5 µm and 0.3 µm respectively. Fig. 15 shows the change in Helmholtz energy during wetting and the physical barriers given by the maxima of the cavities count curves.

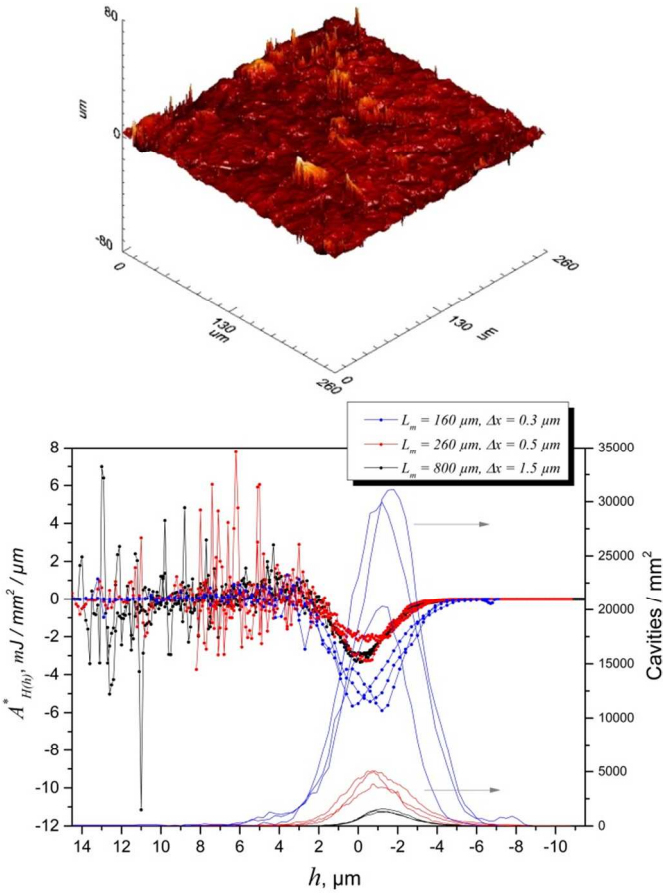

Fig. 15 Above: topographic map of a PP surface modified by a sandpaper of grain 600. Below: change of Helmholtz energy during wetting, and physical barriers given by the maximum cavity count. The curves correspond to three different measurement conditions applied on three different regions of topographic measurements by confocal microscopy on the modified PP surface.

As mentioned above, the physical barriers are given by the maximum cavities count curve. This curve counts the air pockets that would remain dry under the liquid contact line. At the beginning of the contact between liquid-solid, there is only one dry cavity (the whole surface). During wetting, this cavity gets more and more fractioned until it reaches a maximum value of small cavities (Fig. 16). From this point on, if the surface morphology allows it, the number of cavities decreases as the liquid displaces the air out of the pores. In most isotropic surface morphologies, the displacement of air from the pockets is not at all possible: usually, at the height level that contains the maximum number of cavities, i.e. between the mean height

and Z_{min} of random surfaces, the liquid reaches a physical barrier that would only be overcome by compressing the air or by displacing micro bubbles. This maximum of the curve is the physical barrier of wetting for porous surfaces.

The experimental contact angles were determined under controlled laboratory conditions (23°C ± 1°C and 50% ± 4% relative humidity), with 10µL drops of deionized water and using the digital goniometers OCA 35 XL (Data Physics Instruments GmbH, Germany) and FibroDat 1122 (Fibro Systems AB, Sweden). The first instrument was used to measure advancing and receding contact angles, during volume increases and decreases of 0.25 µL/s starting with a droplet of 3 µL, and recorded with a video capture of 3 frames per second. The second instrument was used to measure the static contact angle of a 10 µL drop water after 20 seconds of contact, to give it time to release the mechanical energy used to put a drop on the surface by a small stroke pulse [19].

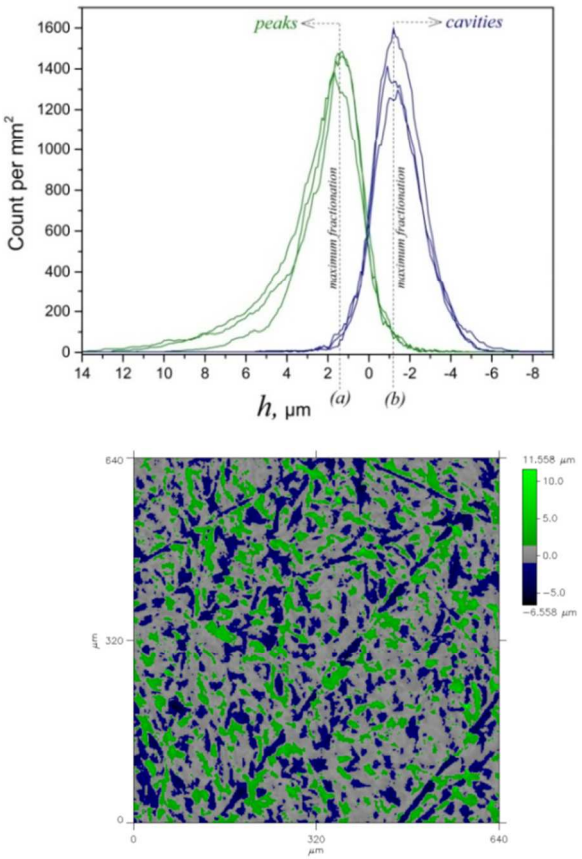

Fig. 16 Peaks and cavities count curves for the surfaces in Fig. 15, using a lateral resolution of 1.5 µm. The counts are expressed per square millimetre of projected surface.

Fig. 17 compares the advancing contact angles measured by the OCA 35 XL device and the static contact angles obtained by the FibroDat 1122 with the values predicted by the model thus making $\phi = \theta_Y + \alpha$, Eq. (13).

The vertical error bars on each experimental and calculated point in Fig. 17 correspond to five contact angle measurements and three topographic maps for each surface respectively. The intermediate scale corresponding to 60X (L_m = 260 µm, Δx = 0.5 µm) can be successfully used to predict the contact angles found experimentally (red dots). The scale 20X (L_m = 800 µm, Δx = 1.5 µm), black dots, results in lower predicted angles than the experimental results, while the finer scale of 100X (L_m = 160 µm, Δx = 0.3 µm), blue dots, predicts greater angles, particularly in the rougher surfaces. The calculation of the contact angles at metastable equilibrium is highly dependent on the measured area and the lateral and vertical resolutions. This fact does not mean that higher resolutions led to more accuracy in the calculation of contact angles. The scale of the roughness that controls wetting depends on the material morphology and also on the liquid properties, such as its viscosity and surface tension.

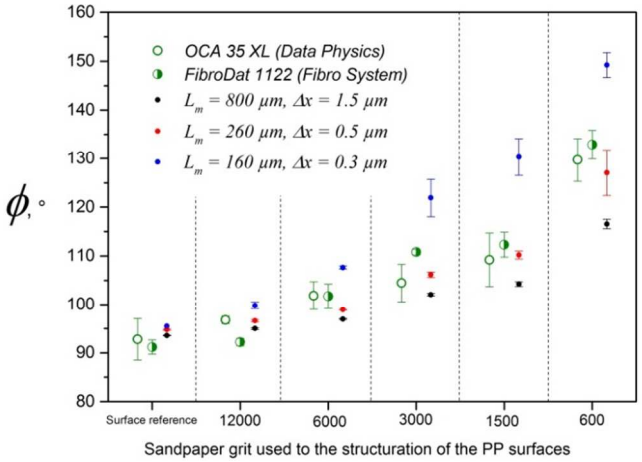

Fig. 17 Apparent contact angles measured using digital goniometers and those predicted by the thermodynamic model.

Recently, Im et al. [18] fabricated regular trapezoidal microstructures using polydimethylsiloxane (PDMS). The resulting geometrical elements were 26 µm in diameter, 11.9 µm in height and 56 degrees in edge's slope, and were molded in square arrays with 40 µm distance between the trapezoidal centres. The authors investigated the wetting properties and the effect of coating the surface with a thin Teflon layer.

In the present study, the microstructure of the elements fabricated lithographically by Im et al. have been digitally reconstructed based on the information and on the EM photographs provided in their article. This was done using surfaces made of tiny squares (Fig. 18) in an arrangement of 10 x 10 trapezoidal elements, L_m = 440 µm, by means of Houdini FX 13.0.314 software (Side Effects, Canada). This surface was then transformed into a map of triangles (138.100 vertices and 269.202 planes) using the 3D Object Converter 4.60 (3doc, Hungary) and OriginPro 9.1 (OriginLab Corporation, USA) software. In order to be consistent with the information provided by Im et al., a height value of zero was assigned to Z_{min}. The WTS of this polygonal map was calculated using algorithms specially designed in the present study for complex 3D-microstructures, and solved with the MATLAB R2014a software (The MathWorks Inc., USA).

According to the experimental results of Im et al., the trapezoidal PDMS surface has a contact angle with deionized water (γ_{LG} = 72 mN/m) of 135°, with Young's angle being PDMS 116°. After coating the surface with a thin Teflon layer (θ_Y = 122°), the contact angle with water was 153°, while the contact angle with methanol (γ_{LG} = 22.7 mN/m, θ_Y = 68°) resulted in 135°. Im et al. used a Phoenix 300 (SEO Co. Ltd., South Korea) goniometer to measure the apparent contact angles, but unfortunately they did not report nor the volume of the water drops used nor the method used to obtain the Young contact angles.

Table 1 Apparent contact angles measured and predicted by the model

Solid surface	Liquid	ϕ_a measured, ° [18]	ϕ_a predicted, °
PDMS	Water	135	134.7 – 135.1
Teflon	Water	153	140.7 – 152.9
Teflon	Methanol	135	72.1 – 133.6

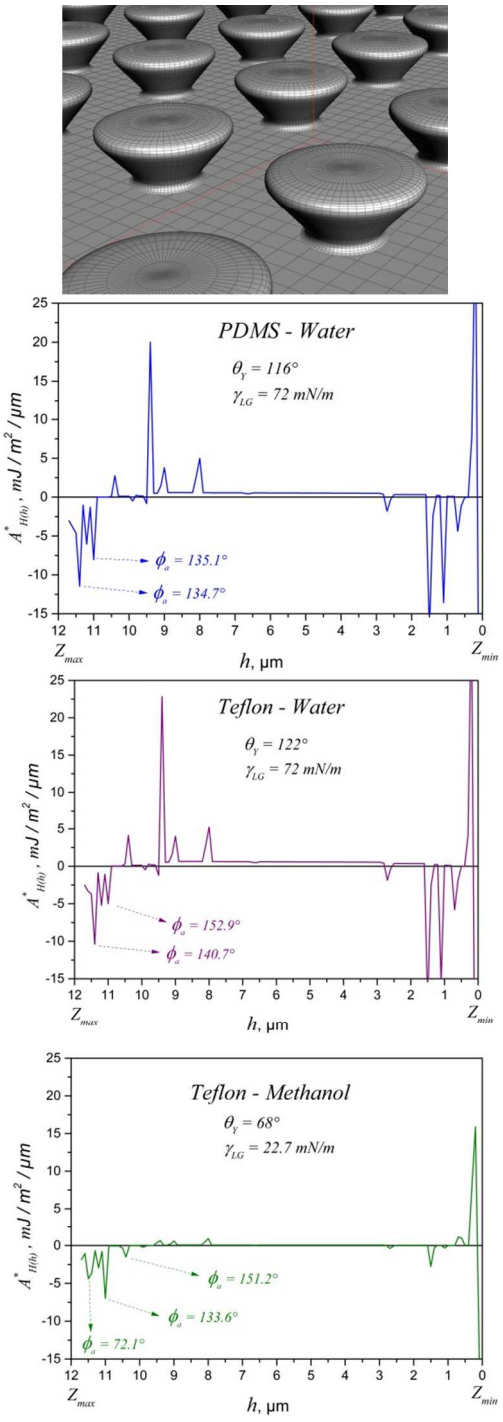

Fig. 18 Results of the wetting simulation of a virtual microstructure similar to the real microstructure used in [18]. The most probable configuration is reached between h = 11.4 and 11.1 µm, just when the liquid wets the first curvature of the trapezoids.

The WTS of the digital surface, the Young's angles and the surface tensions of the liquids, were inputted in the model and yielded satisfactory predictions for the energy barriers and the corresponding apparent contact angles. The results are presented in Table 1 and Fig. 18.

The Helmholtz energy reaches a maximum decrease around the first curvature of the trapezoids. During the first contact, the apparent angles equal Young's angles due to the surface flatness at h = 11.9 µm (see Fig. 19), which can be seen, for example, in the first minimum of the Teflon-Methanol wetting simulation curve in Fig. 18, which corresponds to a predicted contact angle of 72.1° (h = 11.4 µm), very close to the PDMS Young's angle (θ_Y = 68°). However when the liquid reaches h = 11.1 µm, the contact angle increases rapidly due to the curvature of the trapezoid and reaches a value of 133.6°, close to the experimental angle of 135°. A metastable equilibrium is present at around h = 10.4 µm, where the contact angle could be up to 151° (Fig. 18).

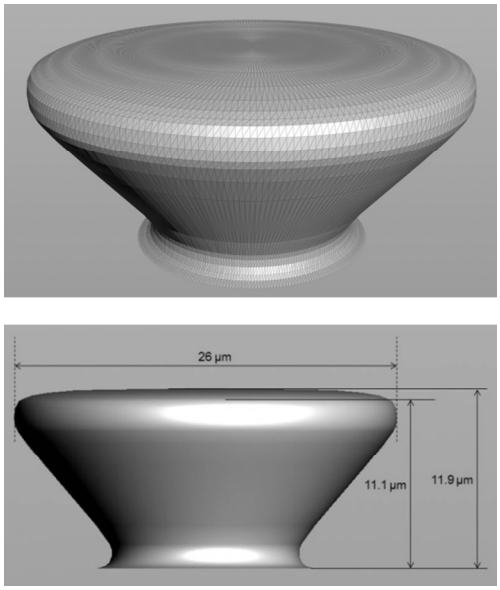

Fig. 19 The trapezoid transformed into a map of triangles (above). Profile and heights of a trapezoid (below). The equilibrium is reached when the wetting of the upper curvature begins.

Im et al. [18] have not reported the standard deviations of their wetting measurements. It would have been interesting to know these values in order to verify that the most probable configuration had been reached in a range of heights and, therefore, that an interval of probable contact angles exist, according to the prediction made by the model. It should be mentioned, that although Im et al. made these microstructured surfaces using modern lithography techniques, it is not possible to obtain completely regularly structured surfaces. Just as the small discontinuity due to the vertices and edges of the virtual polygonal map, the real PDMS surface contains some small texture irregularities due to the moulding and transfer processes. These mathematical and physical irregularities lead to regions of metastable equilibrium for both, the virtual and the real surface, respectively.

These either naturally or artificially structured surfaces, that present inwardly inclined edges and lateral cavities are, as mentioned above, impossible to characterize using current mechanical or optical techniques. However, by constructing virtual polygonal maps, it is possible to study their wetting

properties by calculating and comparing the increase of their surface areas during the process.

Fig. 20 shows how the surface area increases with depth, for different digitally generated polygonal surfaces, the first five using Houdini FX 13.0.314 (Side Effects Software Inc., Canada) and the last by GeoDict 2012 R1(Math2 Market GmbH, Germany). The *Random* surface has already been presented and analysed above. The *Trapezoid* surface is the digital version of the surface Im et al. [18], while *Fractal 1* is a thin flaky surface and *Fractal 2* is a surface of rigidly inclined microfilaments; the *Lotus cluster* is a structure of microspheres in a third-order fractal system, while *Microfiber* is a woven plain fabric constructed using yarns of 200 octagonal profiled filaments. According to Fig 19, the *Lotus cluster* and *Microfiber* surfaces present greater structural depth and, therefore, higher values of interfacial area. However, during the first microns of liquid penetration (Fig. 21), the *Trapezoid* structure shows a significant initial increase, but a few microns deeper is overcome by the *Lotus* cluster and by *Microfiber*.

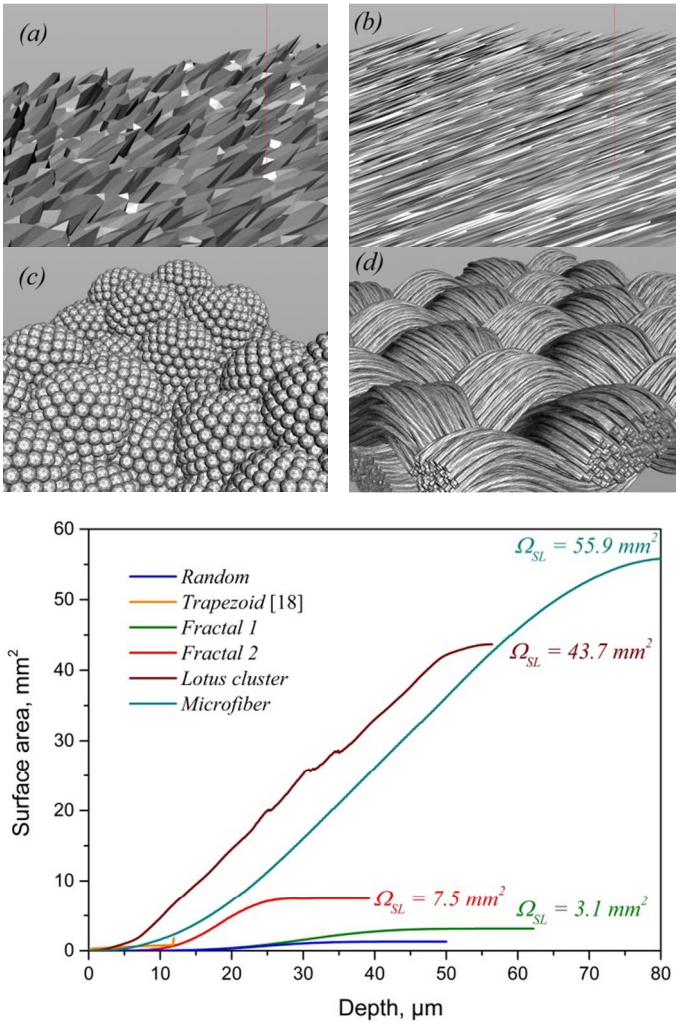

Fig. 20 Increase in the solid-liquid interface area per one square millimetre of projected area, if a liquid wets the surfaces *Fractal 1* (a), *Fractal 2* (b), *Lotus cluster* (c) and *Microfiber* (d). *Lotus cluster* and *Microfiber* have greater depth and higher values of surface area.

However, the *Random* structure, the only one without interstitial cavities, shows a comparatively low surface area increase, similar to that of *Fractal 1*, but only in the region near the upper surface. Thus, if the WTS of a surface is available, it would be possible to study the wetting phenomenon for different values of γ_{LG} and θ_Y, even for complex structures, such as those presented above.

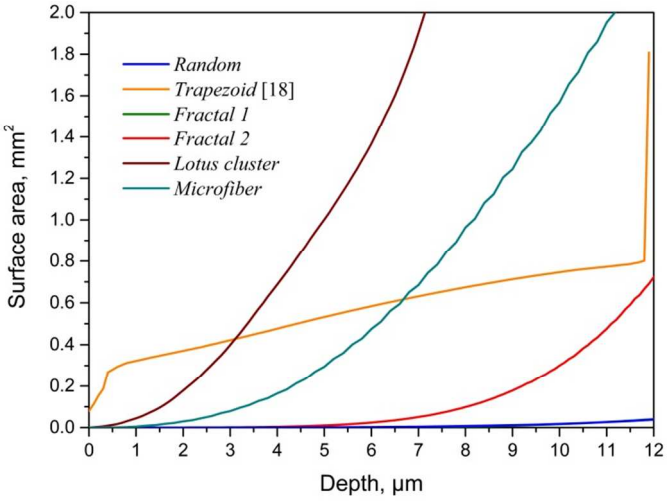

Fig. 21 Increase in the solid-liquid interface area per one square millimetre of projected area during the first microns of depth.

Conclusions

The thermodynamic model presented and tested in this work allows the analysis, understanding and prediction of the wetting phenomena on real and digitally generated topographic maps.

The model considers the solid component as a set of finite elements in the form of small triangular areas. Liquid and gas components are instead evaluated as continuous and incompressible volumes. A major limitation in the use and application of this model is the long computational time required, especially for calculating the WTS, when using small height differentials of topographic maps obtained by high lateral resolution. However, by optimizing the computational algorithms and with the current accelerated hardware and software development, in the future it will probably be possible to improve the computational time.

The most important limitation of this method is that it focuses only the geometrical variability of the surfaces and assumes that the surface is chemically homogeneous.

The calculation of the contact angles at metastable equilibrium is highly dependent on the measured area and the lateral and vertical resolutions. This fact does not mean that higher resolutions led to more accuracy in the calculation of contact angles. The scale of the roughness that controls wetting depends on the material morphology and also on the liquid properties, such as its viscosity and surface tension. The sensitivity of the liquid surface tension and viscosity to the micro, sub-micro and nano-texture presents an interesting field to study for the future.

It is important to note the fundamental considerations that were necessary for the development of the thermodynamic model of wetting presented in this study:

1. The solid-liquid-gas system is bounded by the walls of a small volume of size L_m x L_m x (Z_{max} - Z_{min}), where L_m is the length of the topographic map, Z_{max} is its maximum height and Z_{min} its minimal height.

2. The liquid is one component, and the solid is insoluble in the liquid.
3. The system is located in a small volume underneath the drop, in the contact region between the droplet, the surface and the air filling the cavities.
4. The system is open to the entry of water from the upper face, and the outflow of water and air through the side walls is possible as long as the air is not trapped inside the cavities of the solid.
5. The surface roughness, both in amplitude and distance between asperities, is negligible compared to the radius of the drop.
6. The mass of the fluid within the system volume is negligible and the drop volume very small. Thus, the gravitational force plays no role in the model. Only the cohesive forces of the liquid, which determine its surface tension, and the interfacial energies solid-liquid and solid-gas are the ones that determine the intrinsic contact angle of the system.
7. The apparent contact angles formed in the contact line solid-liquid-gas are controlled by the surface edges and by Young's angle.
8. During the wetting, the liquid moves uniformly from top to bottom regardless of the variations in slope between points at the same contour height. This idealization is the most sensitive of the model, especially in the case of random surfaces.
9. The apparent contact angle for each wetting height is calculated based on the average slope over the whole contour line. This condition compensates the idealization of point 8, by taking all the slopes around the contact line into account.
10. The most probable contact angle -the equilibrium contact angle-, is obtained at the topographic level that presents the greatest change (decrease) of Helmholtz energy.

The handling of the liquid component inside the model could be enhanced by using a three-dimensional mesh model (Eulerian system) [26], a particle model (Lagrangian system) [27], or even better, by the hybridisation of both models as a fluid implicit particle system (FLIP) [28-31]. The use of computational fluid dynamics (CFD) presents an interesting and apparently viable way for performing the model, in order to study and simulate with more accuracy the effects of roughness on the hydrophobic and hydrophilic character of surfaces.

Acknowledgements

The author would like to acknowledge Mrs. Martina Priebs, for her valuable technical support during the dynamic contact angle measurements, to Mr. Benjamin Schur, for his valuable assistance in data processing of the topographic maps and to Dr. Andrea Contreras, for her kind assistance in the final version of this article.

Notes and references

[a] Alfredo Calvimontes, Leibniz-Institut für Polymerforschung Dresden e.V., Hohe Str. 6, 01069 Dresden, Germany. E-mail: calvimontesq@ipfdd.de; Fax +49-351-4658-474; Tel: +49-351-4658-212

1 R.N. Wenzel, Resistance of solid surfaces to wetting by water, *Industrial and Engineering Chemistry*, 1936, **28**, (8), 988-994.
2. A.B.D. Cassie, S. Baxter, Wettability of porous surfaces. *Transactions of the Faraday Society*, 1944, **40**, 546-551.
3. R. Shuttleworth, G. Bailey, The spreading of liquid over a rigid solid, *Discussions Faraday Soc.,* 1948, **3**, 16-22.
4. R.J. Good, A Thermodynamic Derivation of Wenzel's Modification of Young's Equation for Contact Angles; Toghether with a Theory of Hysteresis, *J. Am. Chem. Soc.,* 1952, **74**,504.
5. R.E.. Johnson, R.H., Dettre, Contact Angle and Hsyteresis, in Contact Angle, *Wettability and Adhesion, American Chemical Society*, 1964, USA, pp. 112-135.
6. L. Leger, J.F. Joanny, Liquid Spreading, *Rep. Prog. Phys.,* 1992, 431-436.
7. J.D. Andrade, L.M. Smith, D.E. Gregonis, The Contact Angle and Interface Energetics, in *Surface and Interfacial Aspects of Biomedical Polymers*, 1985, Springer: USA, pp. 249-292.
8. K. Grundke, Wetting, Spreading and Penetration, in *Handbook of Applied Surface and Colloid Chemistry*, (Ed. Krister Holmberg), John Wiley & Sons, Ltd., 2002, pp. 119-141.
9. J. Gaydos,, A.W. Neumann, Line Tension in Multiphase Equilibrium Systems, in *Applied surface thermodynamics*, (E. A.W. Neumann, and Jan K. Spelt), Marcel Dekker, Inc., 1996, New York, USA, pp. 170-238.
10. J. Drelich J., J.D. Miller, Modification of the Cassie Equation. *Langmuir*, 1993, **9**, 619-621.
11. Y.J. Sheng, J. Shaovy, H.K. Tsao, Effects of geometrical characteristics of surface roughness on droplet wetting, *The Journal of Chemical Physics*, 2007, **127**, 234704.
12. C. Ishino, K. Okumura, D. Quéré, Wetting transition on rough surfaces, *Europhys. Lett.,* 2001, **68** (3), 419-425.
13. C.W. Extrand, Model for Contact Angles and Hysteresis on rough and Ultraphobic Surfaces. *Langmuir,* 2002, **18**, 7991-7999.
14. G. Wolansky, A. Marmur, Apparent contact angles on rough surfaces: the Wenzel equation revisited, *Colloids and Surfaces, A: Physicochemical and Engineering Aspects*, 1999, **156,** 381-388.
15. H. Nakae, M. Yoshida, M. Yokota, Effects of roughness pitch of surfaces on their wettability, *Journal of Materials Science*, 2005, **4** (9-10), 2287-2293.
16. T. Kuprenkin, J.A. Taylor, T.M. Schneider, S. Yang, From Rolling Ball to Complete Wetting: The Dynamic Tuning of Liquids on Nanostructured Surfaces, *Langmuir*, 2004, **20** (10, 3824-3827.
17. A. Synytska, L. Ionov, V. Dutschk**,** M. Stamm, K. Grundke, Wetting on Regularly Structured Surfaces from „Core-Shell" Particles: Theoretical Predictions and Experimental Findings, *Langmuir*, 2008, **24**, 11895-11901.
18. M. Im, H. Im, J.H. Lee, J.B. Yoon, Y.K. Choi, A robust superhydrophobic and superoleophobic surface with inverse trapezoidal microstructures on a large transparent flexible substrate. *Soft Matter,* 2010, **6**, 1401-1404.
19. Calvimontes, A. (2011) Topography and the mechanistic understanding of wetting, Südwestdeutscher Verlag für Hochschulschriften, Saarbrücken, Germany.
20. Stout, K.J., Sullivan, P.J., Dong, W.P., Mainsah, E., Luo, N., Mathia, T., Zahouani, H. (1993) The development of methods for the characterisation of roughness in three dimensions, Brussels-Luxemburg: Commission of the European Communities, Brussels-Luxembourg.
21. Volk, R. (2005) Rauheitsmessung: Theorie und Praxis, Beuth Verlag: Germany 2005.
22. Leach, R. (Ed.) (2013) Characterisation of Areal Surface Texture, Springer Verlag: Berlin Heidelberg.

23. Good, R.J., Chaudhury, M.K., Yeung, C. (1998) A new approach for determining roughness by means of contact angles on solids. Mittal Festschrift, 181-197.
24. Calvimontes, A., (2004) *Thermodynamic equilibrium in the wetting of rough surfaces*, Lulu Press Inc., Italy.
25 Ren, W. Wetting Transition on Patterned States and Energy Barriers. *Langmuir*, 2014, **30**, 2879-2885.
26. Jie, T., Xubo, Y. (2009) Physically-based Fluid Animation: a Survey. Sci China Ser F-Inf Sci, 52 (1), 1-17.
27. Salomonsson, F. (2011) PCI/FLIP Fluid Simulation Using A Block-Optimized Grid Data Structure, Department of Science and Technology, Linköping University, Norrköping, Sweden.
28. Williams, B.W. (2008) Fluid Surface Reconstruction from Particles, The Faculty of Graduate Studies in Computer Sciences, The University Of British Columbia, Master of Science Thesis.
29. Brackbill, J.U., Kothe, D.B., Ruppel, H.M. (1988) FLIP: A Low-Dissipation, Particle-In-Cell Method for Fluid Flow. Computer Physics Communications, 48, 25-38
30. Zhu, B., Yang, X., Fan, Y. (2010) Creating and Preserving Vortical Details in SPH Fluid. Pacific Graphics, 29 (7)
31. Cupelli, C.G. (2008) Dissipative Particle Dynamics as Simulation Tool for Capillary Wetting and Suspensions in Microfluidic Applications, Fakultät für Angwandte Wissenschaften der Albert-Ludwigs-Universität Freiburg im Breisgau, PhD. Thesis..